

## Structural Insight into the Stereoselective Inhibition of MMP-8 by Enantiomeric Sulfonamide Phosphonates

Giorgio Pochetti,<sup>†</sup> Enrico Gavuzzo,<sup>†</sup> Cristina Campestre,<sup>‡</sup> Mariangela Agamennone,<sup>‡</sup> Paolo Tortorella,<sup>‡</sup> Valerio Consalvi,<sup>§</sup> Carlo Gallina,<sup>\*‡</sup> Oliver Hiller,<sup>||</sup> Harald Tschesche,<sup>||</sup> Paul A. Tucker,<sup>⊥</sup> and Fernando Mazza<sup>\*‡,¶</sup>

Istituto di Cristallografia, C.N.R., Monterotondo Stazione, Roma, Italy, Dipartimento di Scienze del Farmaco, Università "G. d'Annunzio", Chieti, Italy, Dipartimento di Scienze Biochimiche, Università "La Sapienza", Roma, Italy, Fakultät für Chemie, Abteilung Biochemie I, Universität Bielefeld, Germany, EMBL, c/o DESY, Notkestrasse 85, Hamburg, Germany, and Dipartimento di Chimica, Università di L'Aquila, V. Vetoio, 67010 L'Aquila, Italy

Received August 10, 2005

Potent and selective inhibitors of matrix metalloproteinases (MMPs), a family of zinc proteases that can degrade all the components of the extracellular matrix, could be useful for treatment of diseases such as cancer and arthritis. The most potent MMP inhibitors are based on hydroxamate as zinc-binding group (ZBG).  $\alpha$ -Arylsulfonylamino phosphonates incorporate a particularly favorable combination of phosphonate as ZBG and arylsulfonylamino backbone so that their affinity exceptionally attains the nanomolar strength frequently observed for hydroxamate analogues. The detailed mode of binding of [1-(4'-methoxybiphenyl-4-sulfonylamino)-2-methylpropyl]phosphonate has been clarified by the crystal structures of the complexes that the *R*- and *S*-enantiomers respectively form with MMP-8. The reasons for the preferential MMP-8 inhibition by the *R*-phosphonate are underlined and the differences in the mode of binding of analogous  $\alpha$ -arylsulfonylamino hydroxamates and carboxylates are discussed.

### Introduction

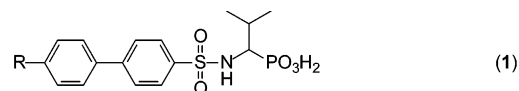
Matrix metalloproteinases (MMPs) comprise a family of zinc endopeptidases that can degrade virtually all the constituents of the extracellular matrix. These enzymes are necessary for normal tissue remodeling and are implicated in some processes such as ovulation, embryonic growth, angiogenesis, differentiation, and healing.<sup>1,2</sup> Overexpression of MMPs activity, however, or inadequate control by the natural tissue inhibitors of MMPs causes degradation of the extracellular matrix in connective tissue,<sup>3</sup> contributing to the pathophysiology of a variety of disease states such as psoriasis,<sup>4</sup> multiple sclerosis,<sup>5,6</sup> osteoarthritis,<sup>7</sup> rheumatoid arthritis,<sup>8,9</sup> osteoporosis,<sup>10,11</sup> and Alzheimer's disease.<sup>12</sup> Excessive MMP activity is critical, in addition, for tumor growth, cancer cell invasion, metastasis, angiogenesis,<sup>13–15</sup> and unwanted degradation of other specific extracellular proteins.<sup>16</sup>

Inhibitors of MMPs are therefore studied for the development of innovative chemotherapeutics in several fields where effective treatments are lacking. A great variety of synthetic, low molecular weight MMP inhibitors have been prepared and tested<sup>17–21</sup> and some of them, such as neovastat, marimastat, and rebimastat, are presently in phase III of clinical trials.<sup>22</sup> Their structures include a peptide or a peptidomimetic moiety that is generally accommodated in the *S'* region of the active site and a zinc-binding group (ZBG) capable of coordinating the catalytic zinc ion.

Hydroxamate is considered, by far, the most effective ZBG. Simple replacement of this function with carboxylate or phosphonate, for example, causes a 100–2000-fold decrease

in potency.<sup>23,24</sup> Hydroxamate inhibitors, however, are generally affected by lack of specificity due to the overwhelming contribution of the hydroxamic group to binding. In addition, they show poor pharmacokinetic properties and may cause toxic effects in long-term treatment owing to the release of hydroxylamine, a well-known carcinogenic compound. Therefore, MMP inhibitors based on less potent zinc-binding functions, such as carboxylate, phosphonate, and thiolate, are also currently investigated. In accordance with these considerations, we have been studying phosphonate MMP inhibitors for a long time,<sup>25–31</sup> with the aim to obtain new potent and selective analogues, endowed with a more favorable pharmacokinetic profile with respect to hydroxamates.

As an extension of our phosphonate program, we were preparing  $\alpha$ -arylsulfonylamino phosphonates (**1**), analogues of known carboxylate<sup>32</sup> and hydroxamate<sup>33,34</sup> MMP inhibitors, when a patent<sup>35</sup> on the same subject appeared. The examples reported in the patent and our own findings ( $K_i$  in the nanomolar range for MMP-2, MMP-3, MMP-8, and aggrecanase) showed that the  $\alpha$ -arylsulfonylamino substitution gives rise to the most potent MMP inhibitors based on phosphonate as ZBG. While the search for new analogues was abandoned, owing to the ample patent coverage, we turned our attention to a stereoselective method of synthesis and to the elucidation of their mode of binding in the active site of MMP-8.



Both enantiomeric forms of  $\alpha$ -arylsulfonylamino phosphonates **1**, similarly to analogous carboxylates and hydroxamates<sup>34,36</sup> (Table 1), are effective MMP inhibitors. The most potent enantiomer is *S* for carboxylates (about 12-fold against MMP-3), *R* for phosphonates (some 1000-fold against MMP-8 and MMP-2), and *R* for hydroxamates (about 100-fold against MMP-3 and MMP-2). It should be pointed out that the priority

\* Corresponding author. Phone: 0039.0871.3555373. Fax: 0039.0871.3555267. E-mail: cgallina@unich.it (C.G.). Phone: 0039.0862.433768. Fax: 0039.0862.433753. E-mail: mazza@univaq.it (F.M.).

<sup>†</sup> Istituto di Cristallografia.

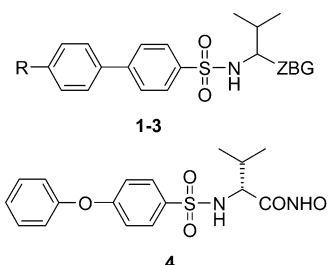
<sup>‡</sup> Università "G. d'Annunzio".

<sup>§</sup> Università "La Sapienza".

<sup>||</sup> Universität Bielefeld.

<sup>⊥</sup> EMBL.

<sup>¶</sup> Università di L'Aquila.

**Table 1.** MMP Inhibition by Enantiomeric  $\alpha$ -Arylsulfonylamino Phosphonates, Carboxylates, and Hydroxamates of the General Formulas


no.	R	ZBG	MMP inhibition (nM)		
			MMP-2	MMP-3	MMP-8
( <i>R</i> )-1	OCH <sub>3</sub>	PO <sub>3</sub> H <sub>2</sub>	5.0 <sup>a</sup>	40.0 <sup>a</sup>	0.6 <sup>a</sup>
( <i>S</i> )-1	OCH <sub>3</sub>	PO <sub>3</sub> H <sub>2</sub>	1200 <sup>a</sup>	< 15% <sup>b</sup>	700 <sup>a</sup>
( <i>R</i> )-2	Br	COOH	5.0 <sup>c</sup>	54.9 <sup>a,d</sup>	ND <sup>e</sup>
( <i>S</i> )-2	Br	COOH	4.0 <sup>c</sup>	4.4 <sup>a,d</sup>	ND
( <i>R</i> )-3	Br	CONHOH	3.0 <sup>c</sup>	8.0 <sup>c</sup>	ND
( <i>S</i> )-3	Br	CONHOH	450 <sup>c</sup>	810 <sup>c</sup>	ND
( <i>R</i> )-4			1.0 <sup>c</sup>	4.0 <sup>c</sup>	ND

<sup>a</sup>  $K_i$  values. <sup>b</sup> At 0.1 mM. <sup>c</sup>  $IC_{50}$  values, pH 7 for MMP-2, pH 6 for MMP-3. <sup>d</sup>  $K_d$  values, pH 6. <sup>e</sup> ND: not determined.

order<sup>37</sup> of substituents at the chiral C $^{\alpha}$  is inverted in phosphonates **1** with respect to carboxylates **2** and hydroxamates **3**. The most potent enantiomers (*R*)-**1** phosphonate and the (*S*)-**2** carboxylate, therefore, bind in the active site with the same orientation of the C $^{\alpha}$  substituents, relative to their ZBG. The most potent hydroxamate, (*R*)-**3**, on the contrary, presents the opposite orientation of the substituents. The stereoselectivity of carboxylates **2** against MMP-3 has been discussed<sup>34,36</sup> and the increased potency of the (*R*)-**3** hydroxamate relative to the *S*-enantiomer was rationalized<sup>34</sup> by molecular modeling based on the crystal structure of MMP-3 complexed with only one of the enantiomers or with structurally related analogues.<sup>38</sup>

To allow reliable determination of the inhibition constants and to attempt cocrystallization with MMP-8, both the (*R*)-**1** and (*S*)-**1** phosphonates were prepared in a high degree of enantiomeric purity (99.8% and 99% ee, respectively). The crystal structure of the complex with the more potent (*R*)-**1** enantiomer was of interest to acquire detailed structural information on the mode of binding of this very potent phosphonate inhibitor and to support molecular modeling for the design of MMP inhibitors with improved potency and

selectivity. The structure solution of the complex with the less potent (*S*)-**1** enantiomer would allow detailed structural insight, entirely based on experimental results, into the stereoselective inhibition of MMP-8 by this model of very effective  $\alpha$ -arylsulfonylamino phosphonate inhibitors.

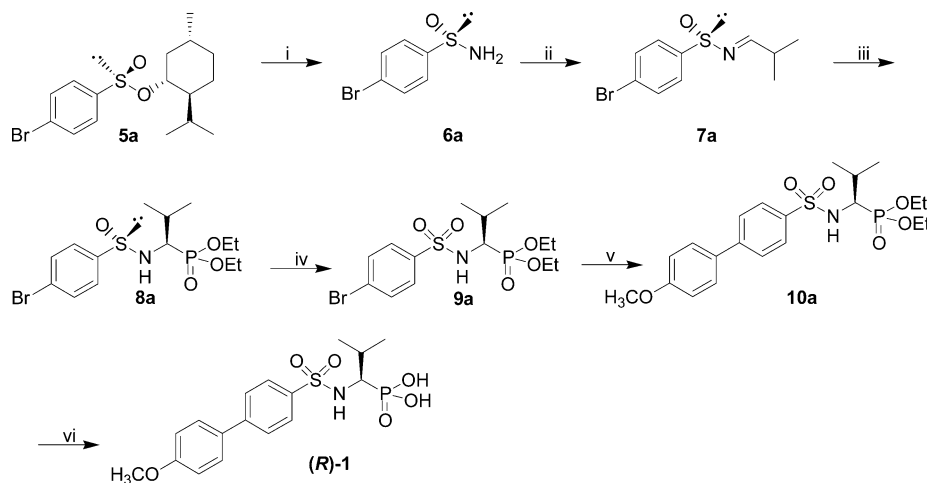
## Results and Discussion

**Chemistry.** The stereoselective method of synthesis for (*R*)-**1** and (*S*)-**1** phosphonates (Scheme 1) was based on asymmetric addition of dialkyl phosphite anions to chiral enantiopure sulfonimines.<sup>39</sup> Addition of lithium bis(trimethylsilyl)amide (LiHMDS)<sup>40</sup> to menthyl (*S*)-*p*-bromobenzenesulfinate **5a**<sup>41</sup> gave the (*S*)-*p*-bromobenzenesulfinamide **6a**, which was converted into the (*S*)-*N*-isobutylidene derivative **7a** by condensation with isobutyraldehyde. Treatment of **7a** with lithium diethyl phosphite afforded the diethyl (*S<sub>S</sub>*,*R*)-*N*-(*p*-bromobenzenesulfinyl)-2-amino-2-methylpropylphosphonate **8a**, which was carefully separated from the minor (*S<sub>S</sub>*,*S*)-diastereoisomer by column chromatography. Oxidation of the (*S<sub>S</sub>*,*R*)-*N*-*p*-bromobenzenesulfinylamide **8a** with *m*-CPBA gave the corresponding (*R*)-*N*-*p*-bromobenzenesulfonylamino phosphonate **9a**, which was coupled<sup>42</sup> with 4-methoxyphenylboronic acid. Acid hydrolysis of the resulting (*R*)-*N*-biphenylsulfonylamino phosphonate **10a** gave the sulfonylamino phosphonate (*R*)-**1** that was purified by crystallization of the cyclohexylamine salt. The enantiomeric purity (99.8% ee) of the phosphonate (*R*)-**1** was monitored by HPLC analysis of the corresponding methyl ester on a Chiralpack AD column. The (*S*)-**1** enantiomer was obtained accordingly, starting from menthyl (*R*)-*p*-bromobenzenesulfinate **5b**, through the enantiomeric intermediates **6b**–**10b**.

**Crystal Structures of MMP-8 Complexed with (*R*)-**1** and (*S*)-**1** phosphonates.** To compare the mode of binding of the two enantiomers with MMPs, the (*R*)-**1** and (*S*)-**1** phosphonates were cocrystallized with MMP-8. Crystals of the complexes, denoted as MMP-8:(*R*)-**1** and MMP-8:(*S*)-**1**, were grown as described in the Experimental Section, where the structure solution and refinement are listed. Figures 1 and 2 show the  $2F_o - F_c$  electron density maps of the *R*- and *S*-enantiomers, complexed in the active site of MMP-8.

Common features of the binding of both inhibitors are occupation of the primed region of the active site, coordination of the catalytic zinc ion by the phosphonate group, and insertion of the biphenyl substituent into the deep primary specificity pocket S<sub>1</sub>'. The two enantiomers, however, adopt different

## Scheme 1<sup>a</sup>



<sup>a</sup> (i) LiHMDS, THF,  $-78$  °C; (ii) isobutyraldehyde, Ti(OEt)<sub>4</sub>, CH<sub>2</sub>Cl<sub>2</sub>, reflux; (iii) lithium diethyl phosphite, THF,  $-78$  °C; (iv) *m*-CPBA, CH<sub>2</sub>Cl<sub>2</sub>, 0 °C; (v) 4-methoxyphenylboronic acid, Pd(PPh<sub>3</sub>)<sub>4</sub>, Na<sub>2</sub>CO<sub>3</sub>, H<sub>2</sub>O/toluene, reflux; (vi) AcOH/HCl, reflux.

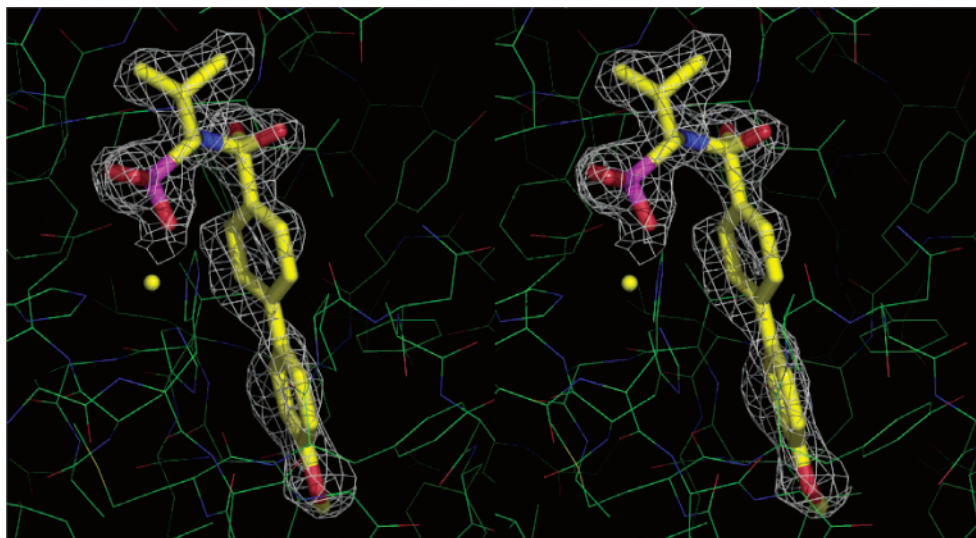


Figure 1.  $2F_o - F_c$  electron density at the active site of MMP-8 with the *R*-enantiomer superimposed. The map is contoured at  $1.0 \sigma$ .

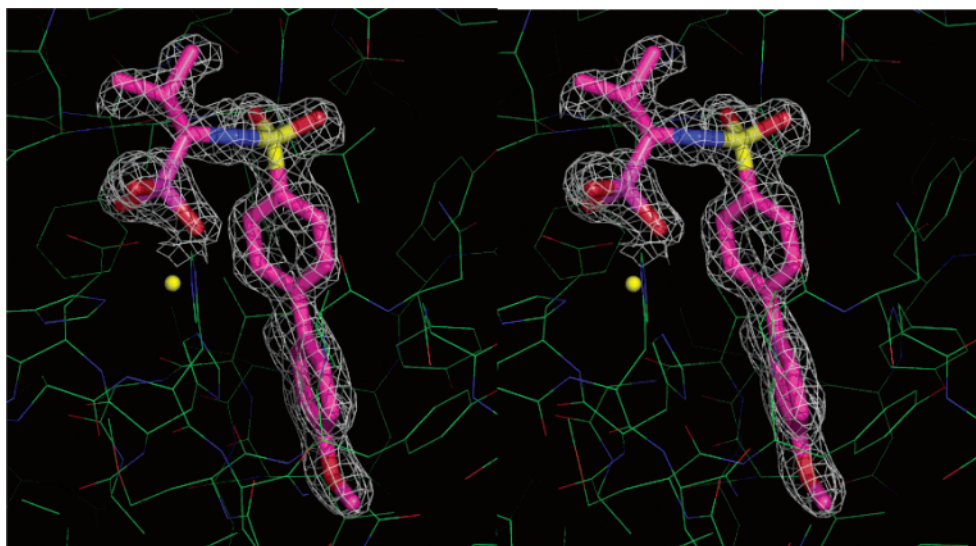


Figure 2.  $2F_o - F_c$  electron density at the active site of MMP-8 with the *S*-enantiomer superimposed. The map is contoured at  $1.1 \sigma$ .

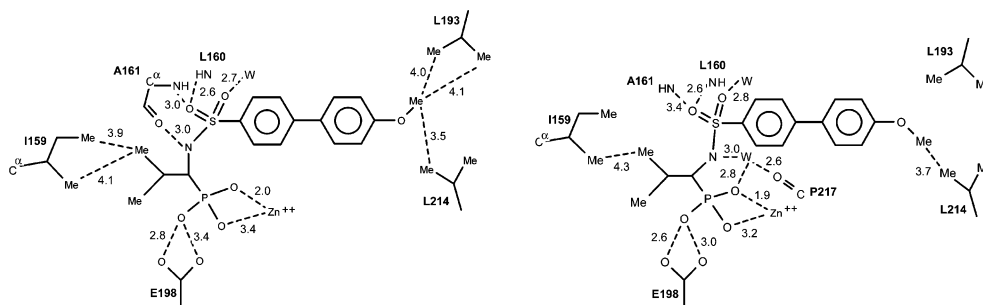


Figure 3. Schematic representation of the binding interactions (dashed lines) of the *R*- (left side) and *S*-enantiomer (right side) at the active site of MMP-8. Distances are in Å.

conformations of the sulfonamide junction and of the lengthy biaryl system. For a better comprehension of the similarities and differences between the mode of binding of the two enantiomers, we have provided their main interactions in the active site of MMP-8 (Figure 3).

**The Phosphonate Coordination.** The coordination of the catalytic zinc ion by the phosphonate group of the two inhibitors is similar. The shortest  $Zn \cdots O$  distance is 2.0 and 1.9 Å for the *R*- and *S*-enantiomer, respectively. The tetrahedral zinc coordination is distorted by the other phosphonate oxygen at 3.4 and 3.2 Å from the metal ion in the *R* and *S* complexed

enantiomer, respectively. The third phosphonate oxygen interacts with the two carboxylate oxygens of the catalytically important E198, forming contacts of 2.8, 3.4 Å and 2.6, 3.0 Å in the MMP-8:(*R*)-1 and MMP-8:(*S*)-1 complex, respectively.

Similar ligations between the catalytic zinc ion and oxygen atoms bound to phosphorus-containing inhibitors have been found in the crystal structures of complexes formed by thermolysin,<sup>43,44</sup> carboxypeptidase A,<sup>45</sup> astacin,<sup>46</sup> and neutrophil collagenase.<sup>27</sup> The exceptional affinity of *R*- $\alpha$ -arylsulfonylamino phosphonates cannot, therefore, be attributed to a particularly effective zinc coordination of the ZBG.

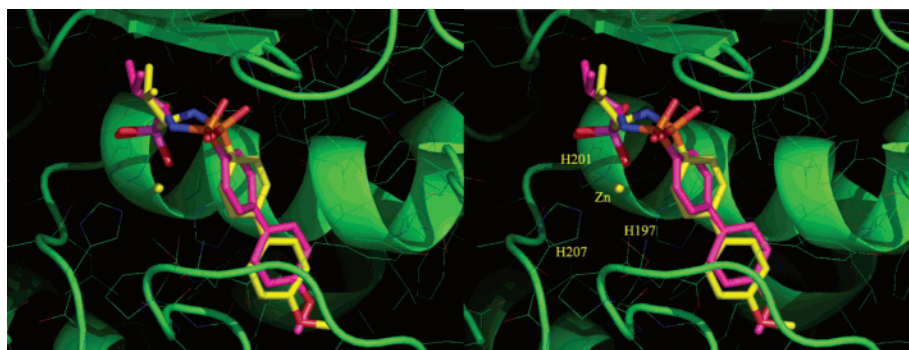


**Figure 4.**  $C^{\alpha}$  superposition of the MMP-8:(*R*)-1 and MMP-8:(*S*)-1 complexes. The the *R*- and *S*-enantiomers are yellow and purple, respectively.

**Binding at the  $S_1$  Pocket.** Despite the opposite chirality at the  $C^{\alpha}$  of the two enantiomers, their isopropyl side chains are located in the same area of the MMP-8  $S_1$  pocket. There, the isopropyl group forms hydrophobic interactions with the I159 side chain protruding from the upper rim formed by the antiparallel  $\beta_4$  strand.<sup>47</sup> Energetically more favorable methyl–methyl interactions are realized by the *R*-enantiomer, since one of its methyls forms contacts of 3.9 and 4.1 Å with both the I159 methyl groups, while only one methyl–methyl contact of 4.3 Å is formed by the *S*-enantiomer.

It is worth noting that also both enantiomers of an *N*-arylsulfonyl tryptophan inhibitor, complexed in the structurally related active site of MMP-3,<sup>38</sup> accommodate the bulky indole rings of Trp in the same area of the  $S_1$  pocket, regardless of the opposite chirality.

**The Sulfonamide Junction.** Search for crystal structures of ligands containing the sequence C–NH–SO<sub>2</sub>–C, performed on the Cambridge Structural Database and PDB, shows that the sulfonamide junction is unlikely to adopt a *trans* conformation. Several crystallographic investigations show the preference for the *gauche* conformations.<sup>48–51</sup> In accordance, the two complexed *R*- and *S*-enantiomers adopt the  $g^+$  (72°) and  $g^-$  (–89°) conformation, respectively. As a consequence, while the sulfonamide NH group of the *R*-enantiomer is turned toward the upper rim, giving rise to a H-bond (3.0 Å) with the A161 CO group, the same NH of the *S*-enantiomer faces the solvent, engaging a H-bond (3.0 Å) with a water molecule. This water is further bridged to an oxygen of the phosphonate and to the P217 CO group. Moreover, in both complexes, one of the sulfonamide oxygens is engaged in a bifurcated H-bond with the L160 and A161 NH groups. The H-bonds engaged by the two enantiomers with L160 have the same strength (2.6 Å). The other H-bond formed by the *R*-enantiomer with the A161 NH group (3.0 Å) is stronger than that engaged by the *S*-enantiomer (3.4 Å). It is worth noting that among the contacts normally anchoring substrate-like inhibitors to the primed region of MMP-8<sup>52–58</sup> the H-bond formed by the L160 NH group is always conserved.

The easy interconversion between the two sulfonamide *gauche* conformations plays a key role for accommodation of both enantiomers in the MMP-8 active site. In fact, the  $g^+$  binding conformation of the (*R*)-1 phosphonate nearly overlaps the  $g^-$  binding conformation of the *S*-enantiomer (Figure 4), allowing the phosphonate to ligate properly the catalytic zinc ion, while the biphenyl group is inserted into the primary specificity pocket  $S_1'$ .

Analogous *gauche* conformations of the sulfonamide junction and similar H-bonding interactions with the protein have also been found in the crystal complexes formed by MMP-3 with the two enantiomers of an *N*-arylsulfonyl tryptophan inhibitor.<sup>38</sup>

**Table 2.** Distances between Ring Centroids and Angles between Ring Mean Planes for the *R*- and *S*-Enantiomer Found in the Crystal Complexes with MMP-8<sup>a</sup>

	$\Phi_p$ –H (Å)	$\Phi_d$ –H (Å)	$\Phi_p$ –H (deg)	$\Phi_d$ –H (deg)	$\Phi_p$ – $\Phi_d$ (deg)
( <i>R</i> )-1	4.1	4.1	12.9	9.1	19.0
( <i>S</i> )-1	4.6	3.9	30.4	10.6	37.0
( <i>R</i> )-4	4.7		34.1		

<sup>a</sup>  $\Phi_p$  and  $\Phi_d$  indicate the proximal and distal phenyl plane of each inhibitor, while H indicates the imidazole H197 ring plane. The last row reports the values relative to the proximal phenyl ring of (*R*)-4 as found in the complex with MMP-3.

Unlike phosphonates, the *R*- and *S*-carboxylates adopt the  $g^-$  and  $g^+$  conformations, respectively, but inversion of the preference for the *gauche* conformation is only apparent.<sup>59</sup>

**Binding at the  $S_1'$  Pocket.** One of the common assumptions in structure-based drug design of enzyme inhibitors is that a chemical moiety that binds tightly, such as the  $P_1'$  biphenyl substituent in the present case, will exhibit the same interacting mode throughout a series of inhibitors. As matter of fact, the crystal structures of the complexes formed by MMP-3 with a series of sulfonamide inhibitors, all containing the biphenyl piperidine substituent,<sup>38</sup> show that the positions of these long ring systems into the deep  $S_1'$  pocket are almost identical. Contrary to these results, a different behavior of the biphenyl moiety into the  $S_1'$  pocket of MMP-8 has been observed. The different penetration and noncoaxial alignment of this lengthy aromatic moiety cause unlike interactions and induce conformational changes of the biaryl systems of the two enantiomers. A comparison of the binding mode of the two enantiomers in the active site of MMP-8 is shown in Figure 4. The insertion of the biphenyl group is deeper for the *R*- than the *S*-enantiomer. The zinc-coordinated H197 imidazole ring, forming a wall of the pocket, is almost halfway between the two phenyl rings of the *R*-isomer. In fact, the centroid of the H197 imidazole ring is equidistant (4.1 Å) from that of both the proximal and distal phenyl ring of the inhibitor (Table 2). Moreover, an almost perfect stacking is realized between these  $\pi$  systems, since the angles formed by the proximal and distal phenyl ring with that of the imidazole are 12.9° and 9.1° (Table 2). This  $\pi$  stacking can reduce the torsion angle around the two aromatic rings of the *R*-isomer to only 19.0°, a value significantly smaller than the average (30°) found for biaryl systems (Cambridge Structural Database).

In the complex of the *S*-enantiomer, only the distal phenyl stacks similarly onto that of H197 (ring centroid distance, 3.9 Å; angle between planes, 10.6°; Table 2). The stack of the proximal phenyl ring is looser (ring centroid distance, 4.6 Å; angle between planes, 30.4°; Table 2). As a consequence, the torsion angle around the two phenyl rings is larger than that of the *R*-enantiomer and attains a value of 37.0°.

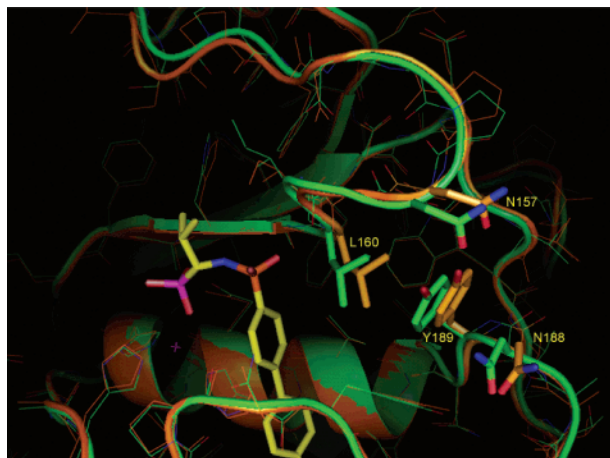


**Figure 5.** Superposition of the enzyme regions 150–160 and 180–189 of complexes MMP-8:(*R*)-1 (orange) and MMP-8:(*S*)-1 (green) obtained by a least-squares fit of the C $^{\alpha}$  atoms of the two complexes. Only the *R*-enantiomer is shown.

The positions of the methoxy oxygen in the two complexed enantiomers differ by ca. 0.8 Å and their methyl groups are oriented in opposite directions. As a consequence, favorable hydrophobic methyl–methyl interactions of 3.5, 4.0, and 4.1 Å (Figure 3) are formed by the *R*-isomer with the surrounding L214 and L193 residues constituting the wall of the pocket. The methoxy of the *S*-enantiomer, on the contrary, is involved in only one methyl–methyl interaction of 3.7 Å, with the L214 residue.

**Inhibitor-Induced Conformational Changes at the Active Site.** Comparison of the crystal structures of the two complexes reveals that the loop regions constituting the active site are quite flexible. In fact, significant conformational changes affect the loops delimiting the S' region, with particular regard to the S $_1$ ' pocket. The largest difference between the corresponding C $^{\alpha}$  atoms of the complexed enzymes is 1.1 Å.

The right-hand side of the active site is bordered by the S-shaped loop connecting the S $_{III}$  to S $_{IV}$  strand and that connecting the S $_V$  strand to the important helix B. Significant differences between the corresponding C $^{\alpha}$  atoms appear for the sequences 150–160 and 180–189 included in the above-mentioned loops. Figure 5 shows a superposition of these regions. The insertion of the *R*-enantiomer pushes aside the L160 residue of the S-shaped loop. This displacement is then propagated to the other residues of the two loops with a concerted mechanism maintaining their H-bonding networks.

The other significant change occurs at the bottom of the primary specificity pocket S $_1$ '. The corresponding C $^{\alpha}$  atoms of the complexed enzymes presenting significant differences are in the region 210–216, containing the so-called "Met turn", and 220–228 ending in the terminal helix-C. These two facing regions separate the crevice harboring the inhibitor biphenyl substituent from bulk water. Figure 6 is a bottom view of the S $_1$ ' pocket showing a superposition of the conformationally different regions.

When the *S*-enantiomer is complexed, the R222 N $^H$  and P211 CO groups form a H-bond (2.7 Å), whereas the *R*-enantiomer causes a displacement (3.8 Å) of these groups and rupture of the intramolecular H-bond. In the latter case, the R222 N $^H$  forms an intermolecular H-bond with the side-chain carboxylate of the symmetry-related D115. It could be argued whether the rupture of the intramolecular H-bond formed by R222 NH could be an artifact of the crystal packing rather than an intrinsic property of the molecular complex. An accurate examination

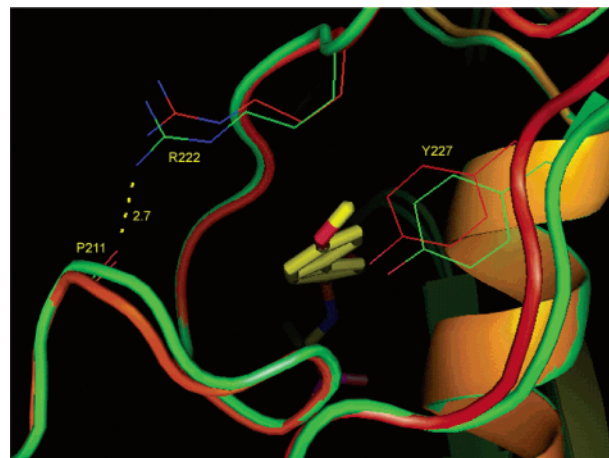


**Figure 6.** Bottom view of the S $_1$ ' pocket showing the superposition of the regions 210–216 and 220–228 of the complexes MMP-8:(*R*)-1 (orange) and MMP-8:(*S*)-1 (green). Only the *R*-enantiomer is shown. The P211 CO and R222 NH groups, giving rise to H-bond only in the MMP-8:(*S*)-1 complex, are indicated. The superposition has been obtained as indicated in Figure 5.

of MMP-8 crystal complexes available from PDB shows that R222 NH is always engaged in intramolecular H-bond with residues 211, 212, or 213 whenever the ligands occupy only the upper part of the S $_1$ ' pocket. On the other hand, in the crystal of MMP-8 complexed with a biphenylsulfonfylamino tetrahydroquinolin carboxylate<sup>27</sup> (Tic) inhibitor (PDB ID 1I76), the R222 NH intramolecular H-bond is also released. In particular, the distal phenyl ring of the Tic derivative is at the same depth of that of the *R*-enantiomer and both are deeper than the distal phenyl of the *S*-enantiomer. Since the MMP-8:(*R*)-1 and MMP-8:Tic complexes present different unit cell parameters and crystal packing, rupture of the intramolecular H-bond formed by R222, rather than an artifact, appears to be the consequence of steric strain due to deeper insertion of the biphenyl substituents.

**Structure-Activity Relationship.** The activity against MMP-8 of the *R*-phosphonate ( $K_i = 0.6$  nM) is more than 1000-fold higher than that of the *S*-enantiomer ( $K_i = 0.7$  μM). By comparison of the crystal complexes, binding interactions that increase the potency of the *R*-inhibitor can be summarized as follows: (i) the *R*-enantiomer promotes better hydrophobic interactions of the isopropyl side chain at the S $_1$  subsite; (ii) the direct inhibitor to protein H-bond, between the sulfonamide NH of the *R*-enantiomer and the A161 CO, is replaced with a water-mediated H-bond to the P217 CO by the *S*-enantiomer; (iii) the bifurcated H-bond between the sulfonamide oxygen and the A161 NH is stronger for the *R*-isomer; (iv) increased  $\pi$ -stacking and more extensive hydrophobic interactions in the S $_1$ ' pocket are due to the deeper insertion of the *R*-inhibitor.

Enantiomeric sulfonamide carboxylates and hydroxamates have been studied as MMP-3 inhibitors. Since the active sites of MMP-3 and MMP-8 are structurally related, the mode of binding and stereoselectivity of these ligands can be compared to that of (*R*)-1 and (*S*)-1 phosphonates. Carboxylate enantiomers show a low level of stereoselectivity against MMP-3. In fact, the *S*-enantiomers of *N*-arylsulfonyl tryptophan<sup>38</sup> and *N*-arylsulfonyl valine<sup>34,36</sup> have  $K_i$  values ca. 2 and 12-fold lower than their *R*-isomers, respectively. The crystal structures of the Trp enantiomers complexed with MMP-3 show that the small decrease in affinity of the *R*-enantiomer is mainly caused by the lack of the inhibitor–protein H-bond, occurring when the sulfonamide NH is turned toward the bulk solvent. Since crystal complexes containing the Val derivatives could not be obtained, isothermal titration calorimetry allowed to assert that the

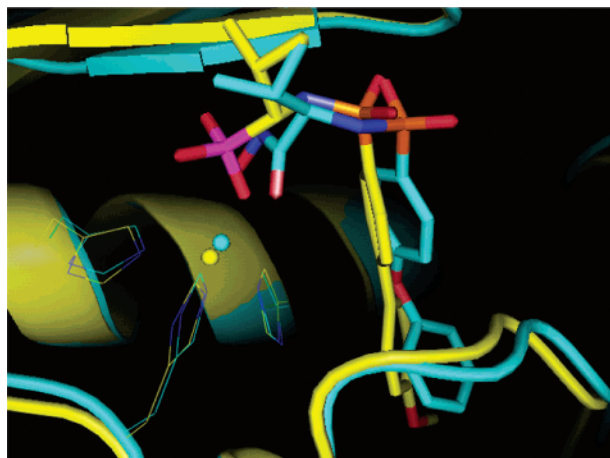


**Figure 7.** C $\alpha$  superposition of the MMP-8:(*R*)-1 (yellow) and MMP-3:(*R*)-4 (cyan) complexes.

higher binding affinity of the *S*-enantiomer should be attributed to conformational entropy factors.<sup>36</sup>

Hydroxamates present opposite stereoselectivity with respect to carboxylates, and the (*R*)-3 potency against MMP-3 is more than 160-fold higher than that of (*S*)-3. Crystals of the complexes between MMP-3 and the hydroxamates (*R*)-3 and (*S*)-3 could not be obtained, but it was possible to crystallize the complex of MMP-3 with the hydroxamate analogue (*R*)-4<sup>34</sup> (Table 1), containing a biphenyl ether group at P1'. The four strong interactions of the hydroxamate group with the catalytic zinc ion, combined with the steric requirement of almost coplanarity of their heavy atoms, strongly reduce the possibilities of ligand adaptation in the enzyme active site. Under these circumstances, the *R*-enantiomer can easily accommodate the  $\alpha$ -isopropyl group at S<sub>1</sub>, while the isopropyl of the *S*-enantiomer is predicted to be oriented back, in contact with the  $\beta$ -sheet of the upper rim, with significant loss of binding affinity. In contrast, carboxylate ligands (*R*)-2 and (*S*)-2, forming less strong interactions with the protein, allow an easy reorientation of the side chains, so that both enantiomers occupy nearly the same area in the S<sub>1</sub> subsite, giving rise to a lower degree of stereoselectivity.

(*R*)- $\alpha$ -Arylsulfonylamino phosphonates such as (*R*)-1 are by far the most potent inhibitors containing the phosphonate as ZBG. They attain  $K_i$  values in the nanomolar range, which is usual only for hydroxamates. Moreover, they present opposite<sup>59</sup> stereoselectivity with respect to the analogue hydroxamate (*R*)-3. To rationalize this behavior at molecular level we present in Figure 7 a superposition between the enzyme structural invariants of MMP-8:(*R*)-1 and MMP-3:(*R*)-4 complexes showing the putative position of (*R*)-4 relative to (*R*)-1.

The completely different zinc ligation causes a considerable displacement of the P atom from the hydroxamate C atom. However, the  $\alpha$ -isopropyl groups of both inhibitors almost overlap at the S<sub>1</sub> subsite, despite the opposite orientation of the C $\alpha$  substituents. The hydroxamate (*R*)-4 adopts the sulfonamide g<sup>-</sup> conformation, so that only the sulfonamide NH of phosphonate (*R*)-1 can form the H-bond with the upper rim of the active site. Moreover, although the proximal phenyl rings of (*R*)-1 and (*R*)-4 are almost at the same depth in the S<sub>1</sub>' pocket, that of (*R*)-4 is at 4.7 Å and rotated 34° (Table 1) with respect to the H197 ring, loosening  $\pi$ -stacking interactions. This rotation avoids an eclipsed conformation between the aromatic ring and the SO<sub>2</sub> group. Therefore, the additional H-bond formed by the sulfonamide NH of (*R*)-1 with the protein and the  $\pi$ -stacking of the proximal phenyl ring with H197 can compensate the higher effectiveness of hydroxamate as ZBG, explaining the

exceptional nanomolar potency of the phosphonate (*R*)-1. This study may serve as a structural basis for the design of more selective phosphonate MMP inhibitors in the nanomolar range.

## Conclusions

The modes of binding of the enantiomeric sulfonamide phosphonates (*R*)-1 and (*S*)-1 in the active site of MMP-8 are reported. The higher inhibiting activity of (*R*)-1 ( $K_i = 0.6$  nM) with respect to (*S*)-1 ( $K_i = 0.7$   $\mu$ M) can be related to (i) better hydrophobic interactions at the S<sub>1</sub> subsite by the isopropyl side chain, (ii) an additional H-bond between the sulfonamide NH and the A161 CO, (iii) a stronger H-bond between the sulfonamide oxygen and the A161 NH, and (iv) increased  $\pi$ -stacking and more hydrophobic interactions in the S<sub>1</sub>' pocket because of its deeper insertion.

$\alpha$ -Arylsulfonylamino phosphonates such as (*R*)-1 incorporate a particularly favorable combination of phosphonate as ZBG and arylsulfonylamino backbone so that their affinity exceptionally attains the nanomolar strength frequently observed for hydroxamate analogues. A comparison between the crystal structures of (*R*)-1 complexed with MMP-8 and (*R*)-4 complexed with MMP-3 shows that the additional H-bond formed by the sulfonamide NH with MMP-8 and the  $\pi$ -stacking of the proximal phenyl ring with H197 can compensate the higher effectiveness of hydroxamates as ZBG, explaining the exceptional nanomolar potency of the phosphonate (*R*)-1.

## Experimental Section

**General.** Melting points were determined on a Büchi B-540 apparatus and are uncorrected. Infrared spectra (IR) were run on a Perkin-Elmer 1600 spectrometer. Absorption values are expressed in wavenumbers (cm<sup>-1</sup>). Optical rotations were measured with a Perkin-Elmer 241 digital polarimeter at 20 °C; concentrations are expressed as g/100 mL. <sup>1</sup>H, <sup>13</sup>C, and <sup>31</sup>P NMR spectra were recorded on a Varian VXR 300 spectrometer, operating at 300, 75, and 121 MHz, respectively. Chemical shifts are expressed in  $\delta$  (ppm) values relative to an internal standard (TMS for proton and carbon; H<sub>3</sub>-PO<sub>4</sub> for phosphorus), while coupling constants ( $J$ ) are given in Hz. <sup>13</sup>C and <sup>31</sup>P NMR spectra are fully proton decoupled. Elemental microanalyses of C, H, N were performed on a Carlo Erba model 1106 analyzer and were within  $\pm 0.4\%$  of the calculated values.

**(*S*)-*p*-Bromobenzenesulfonamide (6a).** A solution (1.0 M in THF) of LiHMDS (7.6 mL, 7.6 mmol) was added dropwise, under stirring, to a solution of menthyl (*S*)-*p*-bromobenzenesulfinate **5a**<sup>41</sup> (2.00 g, 5.57 mmol) in THF (13 mL), cooled at -78 °C. The reaction mixture was warmed to room temperature and stirred for 1 h, and the disappearance of **5a** was monitored (TLC). After quenching with saturated NH<sub>4</sub>Cl (10 mL), the product was extracted with EtOAc (45 mL). The organic phase was dried and concentrated to give a solid residue that was crystallized from EtOAc to give 840 mg (68%) of **6a**: [ $\alpha$ ]<sub>D</sub><sup>20</sup> +27.8° (*c* 1.0 CH<sub>3</sub>OH).

**(*S*)-*N*-(2-Methylpropylidene)-*p*-bromobenzenesulfonamide (7a).** Isobutyraldehyde (0.34 mL 3.68 mmol) and titanium(IV) ethoxide (3.95 mL, 18.85 mmol) were added to a solution of **6a** (810 mg, 3.68 mmol) in CH<sub>2</sub>Cl<sub>2</sub> (60 mL), under N<sub>2</sub>. The reaction mixture was refluxed for 3 h and quenched at 0 °C by addition of H<sub>2</sub>O (50 mL). After filtration through a short pad of Celite, the organic phase was secured and the aqueous phase was further extracted with CH<sub>2</sub>-Cl<sub>2</sub> (100 mL). The pooled organic phases were dried and concentrated, leaving the crude product **7a** (875 mg) as a yellow oil that was employed without further purification.

**Diethyl (*S,S,R*)-*N*-(*p*-Bromobenzenesulfinyl)-2-amino-2-methylpropylphosphonate (8a).** To a solution of diethyl phosphite (0.82 mL, 6.36 mmol) in THF (50 mL), contained in a 100-mL two-necked round-bottom flask equipped with a magnetic stirring bar and rubber septum, was added a solution (1.0 M in THF) of lithium bis(trimethylsilyl)amide (6.36 mL, 6.36 mmol) slowly under nitrogen, at -78 °C. After stirring for 20 min, the resulting mixture

was transferred via cannula to a 250-mL two-necked round-bottom flask equipped with a magnetic stirring bar, rubber septum, and nitrogen inlet and containing a solution of sulfinimine **7a** (875 mg, 3.18 mmol) in THF (30 mL), cooled at  $-78^{\circ}\text{C}$ . After 2 h at  $-78^{\circ}\text{C}$ , the reaction was quenched with saturated  $\text{NH}_4\text{Cl}$  (50 mL), the organic layer was secured, and the aqueous phase was further extracted with EtOAc (150 mL). The pooled organic phases were dried and concentrated to give a yellowish oil that was purified by chromatography on silica gel (1–3% isopropyl alcohol in  $\text{CHCl}_3$ ) to afford 998 mg of **8a** (76%) as a white solid:  $[\alpha]_{\text{D}}^{20} +60.3^{\circ}$  (*c* 1.0 EtOAc).

**Diethyl (R)-N-(p-Bromobenzenesulfonyl)-2-amino-2-methylpropylphosphonate (9a)**. To a solution of **8a** (740 mg, 1.79 mmol) in  $\text{CH}_2\text{Cl}_2$  (35 mL) was added *m*-CPBA (802 mg, 3.58 mmol) portionwise, at  $0^{\circ}\text{C}$ . After 0.5 h, the reaction mixture was sequentially washed with saturated solutions of  $\text{Na}_2\text{S}_2\text{O}_3$  (40 mL),  $\text{NaHCO}_3$  (40 mL), and brine. The organic phase was dried and concentrated in vacuo to give 766 mg (100%) of the pure compound **9a** as a white solid:  $[\alpha]_{\text{D}}^{20} -11.6^{\circ}$  (*c* 1.0 EtOAc).

**Diethyl (R)-[1-(4'-Methoxybiphenyl-4-sulfonylamino)-2-methylpropyl]phosphonate (10a)**. A solution of **9a** (650 mg, 1.52 mmol) and 4-methoxyphenylboronic acid (290 mg, 1.91 mmol) in toluene (7 mL) was treated with tetrakis(triphenylphosphine)-palladium(0) (28 mg) and aqueous  $\text{Na}_2\text{CO}_3$  (0.5 g, 5 mL  $\text{H}_2\text{O}$ ). After being refluxed for 70 h, the reaction mixture was diluted with EtOAc (10 mL) and 1 N HCl (10 mL) and filtered through a short pad of Celite. The organic layer was further washed with saturated solution of  $\text{NaHCO}_3$  (15 mL) and brine, dried, and concentrated in vacuo. The resulting yellow oil was purified by chromatography on silica gel (40% EtOAc/hexane, containing 1.0% of AcOH) to afford 595 mg of **10a** (86%) as a white solid:  $[\alpha]_{\text{D}}^{20} -14.4^{\circ}$  (*c* 1.0 EtOAc).

**Enantiomeric intermediates 6b–10b** were obtained as reported for **6a–10a** and gave the same spectral data and physical constants, except optical rotations that were opposite in sign.

**(R)-[1-(4'-Methoxybiphenyl-4-sulfonylamino)-2-methylpropyl]phosphonic Acid, Cyclohexylamine Salt [(R)-1]**. The diethyl ester **10a** (200 mg, 0.44 mmol) was dissolved in a mixture of AcOH (4 mL) and concentrated HCl (8 mL) at the boiling point. After 6 h under reflux, the mixture was concentrated in vacuo and the residue, taken up in EtOAc (30 mL), was washed with 2 N HCl (40 mL) and brine, dried, and evaporated under reduced pressure. The white solid residue was dissolved in  $\text{CH}_3\text{OH}$  and added with a small excess of cyclohexylamine. Evaporation of the solvent gave the cyclohexylamine salt **(R)-1**, which was recrystallized from  $\text{CH}_3\text{OH}/\text{Et}_2\text{O}$ , providing 110 mg (50%) of pure material:  $[\alpha]_{\text{D}}^{20} +2.5^{\circ}$  (*c* 1.0  $\text{CH}_3\text{OH}$ ).

**(S)-[1-(4'-Methoxybiphenyl-4-sulfonylamino)-2-methylpropyl]phosphonic Acid, Cyclohexylamine Salt [(S)-1]**. The product was obtained by following the same procedure described for **(R)-1**, starting from methyl **(R)-p**-bromobenzenesulfinate:  $[\alpha]_{\text{D}}^{20} -2.8^{\circ}$  (*c* 1.0  $\text{CH}_3\text{OH}$ ).

**Enantiomeric Excesses of [1-(4'-Methoxybiphenyl-4-sulfonylamino)-2-methylpropyl]phosphonic Acids (R)-1 and (S)-1**. The enantiomeric purities of the phosphonates were determined by HPLC analysis of the corresponding dimethyl esters on a Chiralpack AD column.

**Dimethyl (R)-[1-(4'-methoxybiphenyl-4-sulfonylamino)-2-methylpropyl]phosphonate**: retention time 15.55 min; 99.8% ee.

**Dimethyl (S)-[1-(4'-methoxybiphenyl-4-sulfonylamino)-2-methylpropyl]phosphonate**: retention time 13.09 min; 99.0% ee.

**Enzyme Assay and Determination of the Inhibition Constants**. Inhibition of the matrix metalloproteinases MMP-2, MMP-3, and MMP-8 has been determined at  $25^{\circ}\text{C}$  in Tris/HCl (50 mM, pH 7.5),  $\text{CaCl}_2$  (5 mM), Brij (0.05%), and  $\text{NaN}_3$  (0.02%) by continuously monitoring the hydrolysis of the fluorescent substrate McaPro-Leu-Gly-Leu-Dpa-Ala-Arg-NH<sub>2</sub> (0.20  $\mu\text{M}$ )<sup>60</sup> by MMP-2, MMP-3, and MMP-8, respectively, after 5 min incubation in the presence of the inhibitors. Reactions were started by addition of the substrates in the cuvette, under continuous stirring. The hydrolysis was followed by measuring the increase in relative

fluorescence at 393 nm (excitation at 328 nm) due to the formation of product. The highest enzyme concentration used in the assays was always lower than  $3.8 \times 10^{-10}$  M. Under these conditions, low enzyme concentration and substrate concentration well below the  $K_m$  values, the substrate consumption is negligible but well measurable, and the reaction proceeds linearly for at least 1500 s. The velocity of enzymatic substrate hydrolysis was determined in the 200–1400 s time interval. Data analysis has been performed by assuming a reversible inhibition with rapid binding of the enzyme to the inhibitor, according to the following equilibrium (eq 1):



In a reaction where an inhibitor I reacts reversibly with an enzyme E and an activity assay is used to study the inhibition, the simple reaction scheme (eq 1), which does not take into account the reaction of E with the substrate S, is valid if [E] variation is negligible upon formation of the ES complex, during the activity assay. This condition is satisfied in our assays, since [S] is much lower than the substrate  $K_m$  and the reaction proceeds without deviation from the linearity during the 1200 s of the assays. In fact, substrate consumption was negligible during the assays used to evaluate the control rate in the absence of inhibitor.

Under these conditions, concentrations of the EI complex formed in the assay are measurable from the residual activity according to eq 2.

$$\text{fractional saturation} = [\text{EI}] = 1 - \frac{V_i}{V_0} = \frac{V_i - V_0}{V_0} \quad (2)$$

In our experiments, values of fractional saturation were reported against the inhibitor concentrations. The nonlinear fitting of the data to a rectangular hyperbola, under the condition that [EI] is between 0 and 1, yields  $K_i$  as the [I] where [EI] = 0.5.

**Purification of the Catalytic Domain of HNC**. The truncated form Met80-Gly242 of the catalytic domain of HNC was expressed in *Escherichia coli* and renatured by dialyzing the inclusion bodies, which were dissolved in 6 M urea/100 mM 2-mercaptoethanol, against a buffer containing 100 mM NaCl, 5 mM  $\text{CaCl}_2$ , 0.5 mM  $\text{ZnCl}_2$ , 5 mM Tris/HCl, pH 7.5, as previously described.<sup>61</sup> The activated enzyme was subsequently purified to apparent homogeneity by hydroxamate affinity chromatography as judged by SDS-PAGE.

**Crystallizations**. Crystallizations were performed by hanging-drop vapor diffusion at  $18^{\circ}\text{C}$ . Hanging droplets were made by mixing 1.5  $\mu\text{L}$  of protein solution (6 mg/mL protein in 5 mM  $\text{CaCl}_2$ , 100 mM NaCl, 0.5 mM  $\text{ZnCl}_2$ , 3 mM MES-NaOH, 0.02%  $\text{NaN}_3$ , pH 6.0), 1  $\mu\text{L}$  of inhibitor solution (1 mM inhibitor in 0.2 M MES-NaOH, 20% MeOH, pH 6.0), and 5  $\mu\text{L}$  of PEG solution [10% (m/v) PEG 6000, 0.2 M MES-NaOH, 0.02%  $\text{NaN}_3$ , pH 6.0]. Droplets were concentrated against a reservoir buffer containing 1.6 M sodium phosphate buffer, 0.02%  $\text{NaN}_3$ , pH 6.0.

**Data Collection**. X-ray data were collected under cryogenic conditions (100 K) at the EMBL outstation, DESY, Hamburg, Germany, using a wavelength of 1.00 Å and a 345 MAR Research image-plate scanner as detector. Before mounting in the nitrogen stream, the crystal was transferred into mother solution containing 35% PEG 400 for few seconds, and then mounted in a rayon loop and flash-frozen. Data were integrated and scaled using the programs DENZO and SCALEPACK.<sup>62</sup> A summary of data collection and processing is given in Table 3.

**Structure Analysis**. A structure of MMP-8 complex (PDB ID 1I76) was used as starting model. Randomly about 10% of all reflections not included in the refinement were set aside for cross-validation analysis by means of  $R_{\text{free}}$ . After several cycles of positional refinement by CNS,<sup>63</sup> followed by isotropic refinement of individual B factors, a  $2F_o - F_c$  map showed electron density clearly defining each inhibitor. Further conventional isotropic refinement, including inhibitor and successive water molecules, resulted in a model with  $R$ ,  $R_{\text{free}}$  of 0.208, 0.244 and 0.210, 0.235 for MMP-8:(R)-1 and MMP-8:(S)-1, respectively.

**Table 3.** Statistics of Crystallographic Data and Refinement

	MMP-8:(S)-1	MMP-8:(R)-1
wavelength (Å)	1.0	1.0
temperature (K)	100	100
cell dimensions (Å)	32.06, 67.88, 70.52	32.71, 54.75, 68.41
resolution range (Å)	30.0–1.56 (1.62–1.56) <sup>a</sup>	30.0–1.87 (1.94–1.87) <sup>a</sup>
space group	P2 <sub>1</sub> 2 <sub>1</sub> 2 <sub>1</sub>	P2 <sub>1</sub> 2 <sub>1</sub> 2 <sub>1</sub>
no. of unique reflctns	21 658	10 210
R <sub>sym</sub> (%)	4.5	7.5
I/σ(I)	20.6 (9.1) <sup>a</sup>	13.0 (2.9) <sup>a</sup>
completeness (%)	95.8 (90.5) <sup>a</sup>	95.0 (88.1) <sup>a</sup>
R-factor (%)	21.0	21.2
R <sub>free</sub>	23.5	25.1
rms bonds (Å)	0.010	0.009
rms angles (deg)	1.341	1.252
no. of water molecules	244	144
no. of protein atoms	1283	1283
no. of inhibitor atoms	26	26
no. of metal ions	4	4

<sup>a</sup> The values in parentheses refer to the outer shell.

The atomic coordinates have been deposited with the Protein Data Bank [PDB code 1ZVX for MMP-8:(R)-1 and 1ZS0 for MMP-8:(S)-1].

**Acknowledgment.** Italian MIUR, Deutsche Forschungsgemeinschaft, Bonn (H.T., Ts 8/37-4), and the Fonds der Chemischen Industrie, Frankfurt (H.T.), have supported the research. We thank Dr. P. M. O'Brien (Pfizer Global Research & Development) for sending us the coordinates of the complex MMP-3:(R)-4.

**Supporting Information Available:** Spectroscopic data, purity data, and combustion analysis data. This material is available free of charge via the Internet at <http://pubs.acs.org>.

## References

- Shapiro, S. D. Matrix metalloproteinase degradation of extracellular matrix: Biological consequences. *Curr. Opin. Cell Biol.* **1998**, *10*, 602–608.
- Whittaker, M.; Floyd C. D.; Brown, P.; Gearing, J. H. Design and therapeutic application of matrix metalloproteinase inhibitors. *Chem. Rev.* **1999**, *99*, 2735–2776.
- Woessner, J. P., Nagase H., Eds. *Matrix metalloproteinases and TIMPs*; Oxford University Press: New York, 2000.
- Holleran, W. M.; Galardy, R. E.; Gao, W. N.; Levy, D.; Tang, P. C.; Elias, P. M. Matrix metalloproteinase inhibitors reduce phorbol ester-induced cutaneous inflammation and hyperplasia. *Arch. Dermatol. Res.* **1997**, *289*, 138–144.
- Hewson, A. K.; Smith, T.; Leonard, J. P.; Cuzner, M. L. Suppression of experimental allergic encephalomyelitis in the Lewis rat by the matrix metalloproteinase inhibitor. *Inflamm. Res.* **1995**, *44*, 345–349.
- Chandler, S.; Coates, R.; Gearing, A.; Lury, J.; Wells, G.; Bone, E. Matrix metalloproteinases degrade myelin basic protein. *Neurosci. Lett.* **1995**, *201*, 223–226.
- Lohmander, L. S.; Hoerrner, L. A.; Lark, M. W. Metalloproteinases, tissue inhibitor, and proteoglycan fragments in knee synovial-fluid in human osteoarthritis. *Arthritis Rheum.* **1993**, *36*, 181–189.
- Ahrens, D.; Koch, A. E.; Pope, R. M.; Stein-Picarella, M.; Niedbala, M. J. Expression of matrix metalloproteinase 9 (96-kd gelatinase B) in human rheumatoid arthritis. *Arthritis Rheum.* **1996**, *39*, 1576–1587.
- Blaser, J.; Triebel, S.; Maasjosthusmann, U.; Romisch, J.; Krahl-Mateblowski, U.; Freudenberg, W.; Fricke, R.; Tschesche, H. Determination of metalloproteinases, plasminogen-activators and their inhibitors in the synovial fluids of patients with rheumatoid arthritis during chemical synoviorthesis. *Clin. Chim. Acta* **1996**, *244*, 17–33.
- Ohishi, K.; Fujita, N.; Morinaga, Y.; Tsuruo, T. H-31 human breast cancer cells stimulate type I collagenase production in osteoblast-like cells and induce bone resorption. *Clin. Exp. Metastasis* **1995**, *13*, 287–295.
- Witty, J. P.; Foster, S. A.; Stricklin, G. P.; Matrisian, L. M.; Stern, P. H. Parathyroid hormone-induced resorption in fetal rat limb bones is associated with production of the metalloproteinases collagenase and gelatinase B. *J. Bone Miner. Res.* **1996**, *11*, 72–78.
- Peress, N.; Perillo, E.; Zucker, S. Localization of tissue inhibitor of matrix metalloproteinases in Alzheimer's disease and normal brain. *J. Neuropathol. Exp. Neurol.* **1995**, *54*, 16–22.
- Folkman, J.; Shing, Y. Angiogenesis. *J. Biol. Chem.* **1992**, *267*, 10931–10934.
- Chang, C.; Werb, Z. The many faces of metalloproteases: Cell growth, invasion, angiogenesis and metastasis. *Trends Cell. Biol.* **2001**, *11*, S37–S43.
- Overall, C. M.; Lopez-Otin, C. Strategies for MMP inhibition in cancer: Innovations for the post-trial era. *Nat. Rev. Cancer.* **2002**, *2*, 657–672.
- Coussens, L. M.; Fingleton, B.; Matrisian, L. M. Matrix metalloproteinase inhibitors and cancer: Trials and tribulations. *Science* **2002**, *295*, 2387–2392.
- Schröder, J.; Wenzel, H.; Tschesche, H. 3D Structure and drug design. *Proteases and their inhibitors in cancer metastasis*; Foidart, J. M., Muschel, R. J., Eds.; Kluwer Academic Publishers: Dordrecht, 2002; pp 127–150.
- Peterson, J. T. Matrix metalloproteinase inhibitor development and the remodelling of drug discovery. *Heart Failure Rev.* **2004**, *9*, 63–79.
- Puerta, D. T.; Cohen, S. M. A bioinorganic perspective on matrix metalloproteinase inhibition. *Curr. Top. Med. Chem.* **2004**, *4*, 1551–1573.
- Matter, H.; Schudok, M. Recent advances in the design of matrix metalloprotease inhibitors. *Curr. Opin. Drug. Discuss.* **2004**, *7*, 513–535.
- Skiles, J. W.; Gonnella, N. C.; Jeng, A. Y. The design, structure, and clinical update of small molecular weight matrix metalloproteinase inhibitors. *Curr. Med. Chem.* **2004**, *11*, 2911–2977.
- Abbenante, G.; Fairlie, D. P. Protease inhibitors in the clinic. *Med. Chem.* **2005**, *1*, 71–104.
- Muri, E. M. F.; Nieto, M. J.; Sindelar, R. D.; Williamson, J. S. Hydroxamic acids as pharmacological agents. *Curr. Med. Chem.* **2002**, *9*, 1631–1653.
- Babine, R. E.; Bender, S. L. Molecular recognition of protein–ligand complexes: Application to drug design. *Chem. Rev.* **1997**, *97*, 1359–1472.
- Cirilli, M.; Gallina, C.; Gavuzzo, E.; Giordano, C.; Gomis-Ruth, F. X.; Gorini, B.; Kress, L. F.; Mazza, F.; Paradisi, M. P.; Pochetti, G.; Politi, V. 2 Angstrom X-ray structure of adamalysin II complexed with a peptide phosphonate inhibitor adopting a retro-binding mode. *FEBS Lett.* **1997**, *418*, 319–322.
- D'Alessio, S.; Gallina, C.; Gavuzzo, E.; Giordano, C.; Gorini, B.; Mazza, F.; Paradisi M. P.; Panini, G.; Pochetti, G.; Sella, A. Inhibition of adamalysin II and MMPs by phosphonate analogues of snake venom peptides. *Bioorg. Med. Chem.* **1999**, *7*, 389–394.
- Gavuzzo, E.; Pochetti, G.; Mazza, F.; Gallina, C.; Gorini, B.; D'Alessio, S.; Pieper, M.; Tschesche, H.; Tucker, P. A. Two crystal structures of human neutrophil collagenase, one complexed with a primed- and the other with an unprimed-side inhibitor: Implications for drug design. *J. Med. Chem.* **2000**, *43*, 3377–3385.
- D'Alessio, S.; Gallina, C.; Gavuzzo, E.; Giordano, C.; Gorini, B.; Mazza, F.; Pagliarlunga Paradisi, M.; Panini, G.; Pochetti, G. Conformationally constrained analogues of endogenous tripeptide inhibitors of zinc metalloproteinases. *Eur. J. Med. Chem.* **2001**, *36*, 43–53.
- Aschi, M.; Roccatano, D.; Di Nola, A.; Gallina, C.; Gavuzzo, E.; Pochetti, G.; Pieper, M.; Tschesche, H.; Mazza, F. Computational study of the catalytic domain of human neutrophil collagenase. Specific role of the S3 and S'3 subsites in the interaction with a phosphonate inhibitor. *J. Comput. Aided Mol. Des.* **2002**, *16*, 213–225.
- Agamennone, M.; Campestre, C.; Preziuso, S.; Consalvi, V.; Crucianelli, M.; Mazza, F.; Politi, V.; Ragno, R.; Tortorella, P.; Gallina, C. Synthesis and evaluation of new tripeptide phosphonate inhibitors of MMP-8 and MMP-2. *Eur. J. Med. Chem.* **2005**, *40*, 271–279.
- Bianchini, G.; Aschi, M.; Cavicchio, G.; Crucianelli, M.; Preziuso, S.; Gallina, C.; Nistri, A.; Gavuzzo, E.; Mazza, F. Design, modelling, synthesis and biological evaluation of peptidomimetic phosphinates as inhibitors of matrix metalloproteinases MMP-2 and MMP-8. *Bioorg. Med. Chem.* **2005**, *13*, 4740–4749.
- Watanabe, F.; Tsuzuki, H.; Ohtani, M. Preparation of *N*-sulfonylamino acid derivatives as metalloproteinase inhibitors. International Patent Application, WO 9727174 A1, 1997.
- Robinson, R. P. Arylsulfonylamino hydroxamic acid derivatives. European Patent Application, EP 895988 A1, 1999.

- (34) O'Brien, P. M.; Ortwine, D. F.; Pavlovsky, A. G.; Picard, J. A.; Sliskovic, D. R.; Roth, B. D.; Dyer, R. D.; Johnson, L. L.; Man, C. F.; Hallak, H. Structure-activity relationships and pharmacokinetic analysis for a series of potent, systemically available biphenyl-sulfonamide matrix metalloproteinase inhibitors. *J. Med. Chem.* **2000**, *43*, 156–166.
- (35) Schudok, M.; Schwab, W.; Zoller, G.; Bartnik, E.; Buttner, F.; Weithmann, K. U. Sulfonylaminophosphinic and sulfonylamino-phosphonic acid derivatives, methods for their preparation and use. Patent US 6,235,727 B1, 2001 and Patent US 6,500,811 B2, 2002.
- (36) Parker, M. H.; Ortwine, D. F.; O'Brien, P. M.; Lunney, E. A.; Banotai, C. A.; Mueller, W. T.; McConnell, P. and Brouillette, C. G. Stereoselective binding of an enantiomeric pair of stromelysin-1 inhibitors caused by conformational entropy factors. *Bioorg Med. Chem. Lett.* **2000**, *10*, 2427–2430.
- (37) Prelog, V.; Helmchen, G. Basic Principles of the CIP-System and Proposals for a Revision. *Angew. Chem., Int. Ed. Engl.* **1982**, *21*, 567–583.
- (38) Pavlovsky, A. G.; Williams, M. G.; Ye, Q. Z.; Ortwine, D. F.; Purchase, C. F., II; White, A. D.; Dhanaraj, V.; Roth, B. D.; Johnson, L. L.; Hupe, D.; Humblet, C.; Blundell, T. L. X-ray structure of human stromelysin catalytic domain complexed with nonpeptide inhibitors: Implications for inhibitor selectivity. *Protein Sci.* **1999**, *8*, 1455–1462.
- (39) Mikolajczyk, M.; Lyzwa, P.; Drabowicz, J. Asymmetric addition of dialkyl phosphite and diamido phosphite anions to chiral, enantiopure sulfinimines: A new, convenient route to enantiomeric  $\alpha$ -amino-phosphonic acids. *Tetrahedron Asymmetry* **1997**, *8*, 3991–3994.
- (40) Davis, F. A.; Zhang, Y.; Andemichael, Y.; Fang, T.; Fanelli, D. L.; Zhang, H. Improved synthesis of enantiopure sulfinimines (thiooxime S-oxides) from *p*-toluenesulfonamide and aldehydes and ketones. *J. Org. Chem.* **1999**, *64*, 1403–1406.
- (41) Capozzi, M. A. M.; Cardellicchio, C.; Naso, F.; Spina, G.; Tortorella, P. Highly stereoselective route to dialkyl sulfoxide based upon the sequential displacement of oxygen and carbon leaving groups by Grignard reagents on sulfinyl compounds. *J. Org. Chem.* **2001**, *66*, 5933–5936.
- (42) Miyuara, N.; Yanagi, T.; Suzuki, A. The palladium-catalyzed cross-coupling reaction of phenylboronic acid with haloarenes in the presence of bases. *Synth. Commun.* **1981**, *11*, 513–519.
- (43) Tronrud, D. E.; Monzingo, A. F.; Matthews, B. W. Crystallographic structural analysis of phosphoramidates as inhibitors and transition-state analogs of thermolysin. *Eur. J. Biochem.* **1986**, *157*, 261–268.
- (44) Holden, H. M.; Tronrud, D. E.; Monzingo, A. F.; Weaver, L. H.; Matthews, B. W. Slow- and fast-binding inhibitors of thermolysin display different modes of binding: Crystallographic analysis of extended phosphoramidate transition-state analogues. *Biochemistry* **1987**, *26*, 8542–8553.
- (45) Kim, H.; Lipscomb, W. N. Crystal structure of the complex of carboxypeptidase A with a strongly bound phosphonate in a new crystalline form: Comparison with structures of other complexes. *Biochemistry* **1990**, *29*, 5546–5555.
- (46) Grams, F.; Dive, V.; Yiotakis, A.; Yiallouris, I.; Vassiliou, S.; Zwilling, R.; Bode, W.; Stocker, W. Structure of astacin with a transition-state analogue inhibitor. *Nat. Struct. Biol.* **1996**, *3*, 671–675.
- (47) Stocker, W.; Grams, F.; Baumann, D.; Reinemer, P.; Gomis-Ruth, F. X.; McKay, D. B.; Bode, W. The metzincins. Topological and sequential relations between the astacins, adamalysins, serralysins, and matrixins (collagenases) define a superfamily of zincpeptidases. *Protein Sci.* **1995**, *4*, 823–840.
- (48) Calcagni, A.; Gavuzzo, E.; Lucente, G.; Mazza, F.; Pochetti, G.; Rossi, D. Structure and conformation of peptides containing the sulfonamide junction. *Int. J. Pept. Protein Res.* **1989**, *34*, 319–324.
- (49) Zecchini, G.; Paradisi, M. P.; Torrini, I.; Lucente, G.; Gavuzzo, E.; Mazza, F.; Pochetti, G. Retrosulfonamido peptide analogues. Synthesis and crystal conformation of Boc-Pro-Leu- $\Psi$ (NH-SO<sub>2</sub>)-Gly-NH<sub>2</sub>. *Tetrahedron Lett.* **1991**, *32*, 6779–6782.
- (50) Calcagni, A.; Gavuzzo, E.; Mazza, F.; Pinnen, F.; Pochetti, G.; Rossi, D. Structure and conformation of peptides containing the sulfonamide junction. IV. Synthesis and crystal conformation of *N*-benzoyl-L-phenylalanyl-tauryl-L-leucine methyl ester. *Gazz. Chim. Ital.* **1992**, *122*, 17–23.
- (51) Calcagni, A.; Rossi, D.; Paglialonga Paradisi, M.; Lucente, G.; Luisi, G.; Gavuzzo, E.; Mazza, F.; Pochetti, G.; Paci, M. Peptides containing the sulfonamide junction: Synthesis, structure, and conformation of Z-Tau-Pro-Phe-NHiPr. *Biopolymers* **1997**, *41*, 555–567.
- (52) Bode, W.; Reinemer, P.; Huber, R.; Kleine, T.; Schnierer, S.; Tschesche, H. The X-ray crystal structure of the catalytic domain of human neutrophil collagenase inhibited by a substrate analogue reveals the essentials for catalysis and specificity. *EMBO J.* **1994**, *13*, 1263–1269.
- (53) Reinemer, P.; Grams, F.; Huber, R.; Kleine, T.; Schnierer, S.; Pieper, M.; Tschesche, H.; Bode, W. Structural implications for the role of the N terminus in the “superactivation” of collagenases. *FEBS Lett.* **1994**, *338*, 227–233.
- (54) Grams, F.; Reinemer, P.; Powers, J. C.; Kleine, T.; Pieper, M.; Tschesche, H.; Huber, R.; Bode, W. X-ray structures of human neutrophil collagenase complexed with peptide hydroxamate and peptide thiol inhibitors. Implications for substrate binding and rational drug design. *Eur. J. Biochem.* **1995**, *228*, 830–841.
- (55) Stams, T.; Spurlino, J. C.; Smith, D. L.; Wahl, R. C.; Ho, T. F.; Qoronfleh, M. W.; Banks, T. M.; Rubin, B. Structure of human neutrophil collagenase reveals large S<sub>1</sub>' specificity pocket. *Nat. Struct. Biol.* **1994**, *1*, 119–123.
- (56) Grams, F.; Crimmin, M.; Hinnes, L.; Huxley, P.; Pieper, M.; Tschesche, H.; Bode, W. Structure determination and analysis of human neutrophil collagenase complexed with a hydroxamate inhibitor. *Biochemistry* **1995**, *34*, 14012–14020.
- (57) Betz, M.; Huxley, P.; Davies, S. J.; Mushtaq, Y.; Pieper, M.; Tschesche, H.; Bode, W.; Gomis-Rüth, F. X. 1.8-Å crystal structure of the catalytic domain of human neutrophil collagenase (matrix metalloproteinase-8) complexed with a peptidomimetic hydroxamate primed-side inhibitor with a distinct selectivity profile. *Eur. J. Biochem.* **1997**, *247*, 356–363.
- (58) Brandstetter, H.; Engh, R. A.; Graf Von Roedern, E.; Moroder, L.; Huber, R.; Bode, W.; Grams, F. Structure of malonic acid-based inhibitors bound to human neutrophil collagenase. A new binding mode explains apparently anomalous data. *Protein Sci.* **1998**, *7*, 1303–1309.
- (59) The geometry of an *R*- $\alpha$ -sulfonylaminophosphonate is superimposable with that of the *S*-carboxylate analogue, owing to the inversion of the priority order of the substituents at C <sup>$\alpha$</sup> .<sup>37</sup>
- (60) Knight, C. G.; Willenbrock, F.; Murphy, G. A novel coumarin-labelled peptide for sensitive continuous assays of the matrix metalloproteinases. *FEBS Lett.* **1992**, *296*, 263–266.
- (61) Schnierer, S.; Kleine, T.; Gote, T.; Hillemann, A.; Knäuper, V.; Tschesche, H. The recombinant catalytic domain of human neutrophil collagenase lacks type I collagen substrate specificity. *Biochem. Biophys. Res. Commun.* **1993**, *191*, 319–326.
- (62) Otwinowski, Z.; Minor, W. Processing of X-ray diffraction data collection in oscillation mode. *Methods Enzymol.* **1997**, *276*, 307–326.
- (63) Brunger, A. T.; Adams, P. D.; Clore, G. M.; DeLano, W. L.; Gros, P.; Grosse-Kunstleve, R. W.; Jiang, J. S.; Kuszewski, J.; Nilges, M.; Pannu, N. S.; Read, R. J.; Rice, L. M.; Simonson, T.; Warren, G. L. Crystallography and NMR system: A new software suite for macromolecular structure determination. *Acta Crystallogr.* **1998**, *D54*, 905–921.

JM050787+